CrossMark

ORIGINAL PAPER

Hydraulic Fracture Growth in a Layered Formation based on Fracturing Experiments and Discrete Element Modeling

Zou Yushi[1] · Ma Xinfang[1] · Zhou Tong[1] · Li Ning[1] · Chen Ming[1] ·
Li Sihai[1] · Zhang Yinuo[1] · Li Han[2]

Abstract Hydraulic fracture (HF) height containment tends to occur in layered formations, and it significantly influences the entire HF geometry or the stimulated reservoir volume. This study aims to explore the influence of preexisting bedding planes (BPs) on the HF height growth in layered formations. Laboratory fracturing experiments were performed to confirm the occurrence of HF height containment in natural shale that contains multiple weak and high-permeability BPs under triaxial stresses. Numerical simulations were then conducted to further illustrate the manner in which vertical stress, BP permeability, BP density(or spacing), pump rate, and fluid viscosity control HF height growth using a 3D discrete element method-based fracturing model. In this model, the rock matrix was considered transversely isotropic and multiple BPs can be explicitly represented. Experimental and numerical results show that the vertically growing HF tends to be limited by multi-high-permeability BPs, even under higher vertical stress. When the vertically growing HF intersects with the multi-high-permeability BPs, the injection pressure will be sharply reduced. If a low pumping rate or a low-viscosity fluid is used, the excess fracturing fluid leak-off into the BPs obviously decreases the rate of pressure build up, which will then limit the growth of HF. Otherwise, a higher pumping rate and/or a higher viscosity will reduce the leak-off time and fluid volume, but increase the injection pressure to drive the HF to grow and to penetrate through the BPs.

Keywords Layered formation · Bedding plane · Hydraulic fracturing · Height containment · Deflection

Abbreviations

Q_t	Pumping rate
μ	Fracturing fluid viscosity
E_h, E_v	Young's moduli parallel and perpendicular to BP
v_h, v_v	Poisson's ratios parallel and perpendicular to BP
T_{0h}, T_{0v}	Tensile strengths parallel and perpendicular to BP
S_{0h}, S_{0v}	Cohesions parallel and perpendicular to BP
$\varphi_{0h}, \varphi_{0v}$	Frictional angles parallel and perpendicular to BP
k_v, k_{BP}	Permeability perpendicular and parallel to BP
$\sigma_{h\max}, \sigma_{h\min}$ and σ_v	Maximum, minimum horizontal and vertical in situ stresses

1 Introduction

Massive hydraulic fracturing is an essential technology for developing unconventional formations (e.g., shale and tight sandstone) because of its low or ultralow matrix permeability. Using this technology, the largest possible hydraulic fracture network (HFN) with sufficient conductivity is expected to be created for transporting hydrocarbon. However, the existence of bedding planes (BPs) (and/or layer interfaces) can significantly affect the hydraulic

✉ Zou Yushi
zouyushi@126.com

1   State Key Laboratory of Petroleum Resource and Engineering, China University of Petroleum, Beijing 102249, China

2   Texas A and M University, College Station, TX, USA

Fig. 1 Microseismic events monitored during a horizontal well fracturing with multi-stage and multi-cluster in the Longmaxi shale formation in Sichuan basin, China: **a** *side* and **b** *top* views. Note that the microseismic events from different stages overlap each other
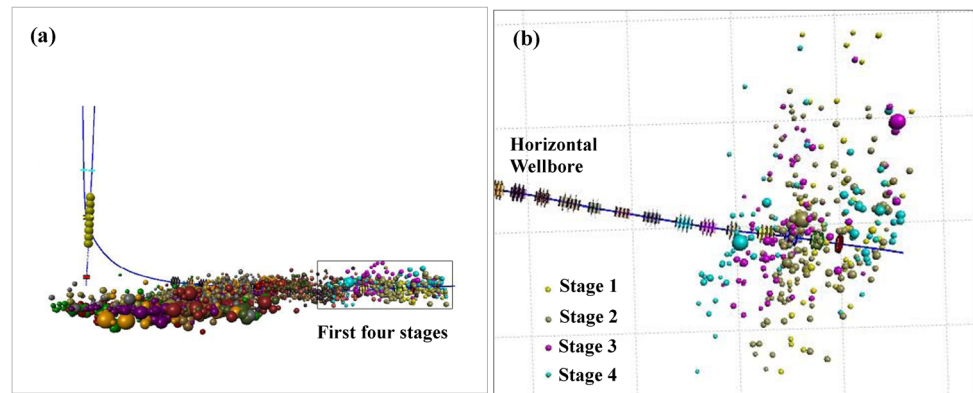

Table 1 Properties of rock mechanics and permeability of shale specimens

| Parameter	Symbol	Units	Value
Young's modulus parallel to BP	E_h	GPa	37.2
Young's modulus perpendicular to BP	E_v	GPa	36.4
Poisson's ratio parallel to BP	v_h	Decimal	0.241
Poisson's ratio perpendicular to BP	v_v	Decimal	0.236
Tensile strength parallel to BP	T_{0h}	MPa	6.7
Tensile strength perpendicular to BP	T_{0v}	MPa	0.0–2.4
Permeability parallel to BP	k_h (k_{BP})	m^2	10^{-19}–10^{-10}
Permeability perpendicular to BP	k_v	m^2	10^{-19}
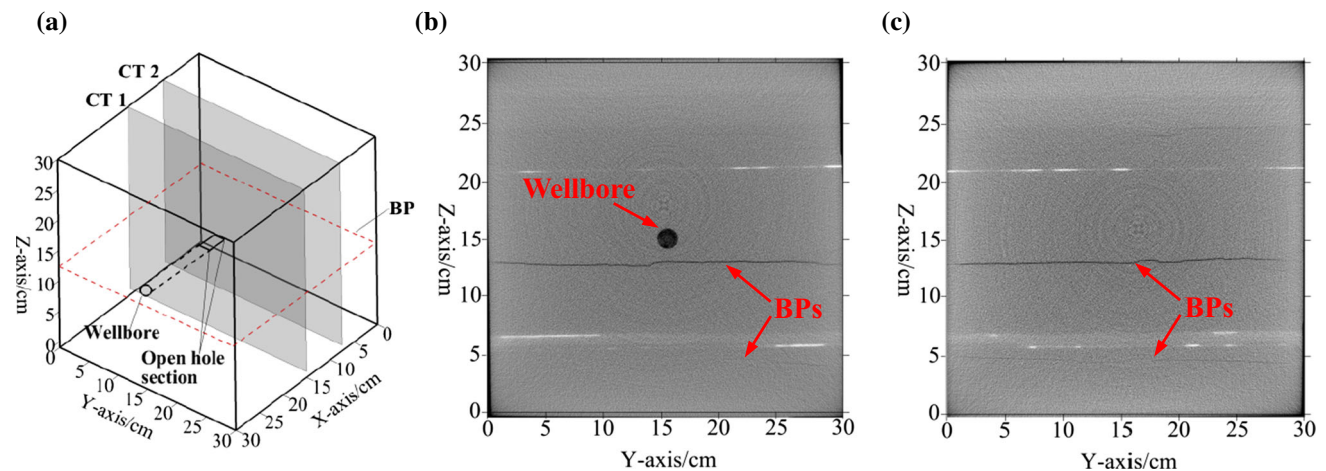
Fig. 2 CT scanning images of preexisting BPs in the specimens before the fracturing experiments: **a** scanning position indicators, **b** CT1, $X = 15.0$ cm, **c** CT2, $X = 22.5$ cm

fracture (HF) growth behavior in some multi-layered formations. The BPs play a significant role in the creation of HFN: On the one hand, BPs may increase the complexity of HFN; on the other hand, BPs may limit HF propagation, particularly its height (Zou et al. 2016a, b). Figure 1 shows the microseismic events monitored during a horizontal well fracturing with multi-stage and multi-cluster in the Longmaxi shale formation in Sichuan basin, China. The result indicates limited HF height growth, and the HFs from

different fracturing stages connect with each other due to the opening of BPs. Hence, understanding the role of BPs in HF complexity and the conditions, under which the HF penetrates through BPs, is significant for the successful design of field stimulation in layered formations.

Given that HF height is one of the critical factors that can determine the success or failure of a fracturing treatment, HF height containment mechanism in layered formations has been extensively investigated (Daneshy 1978;

Fig. 3 Diagram of the cross-sectional view of the laboratory setup for fracturing simulations
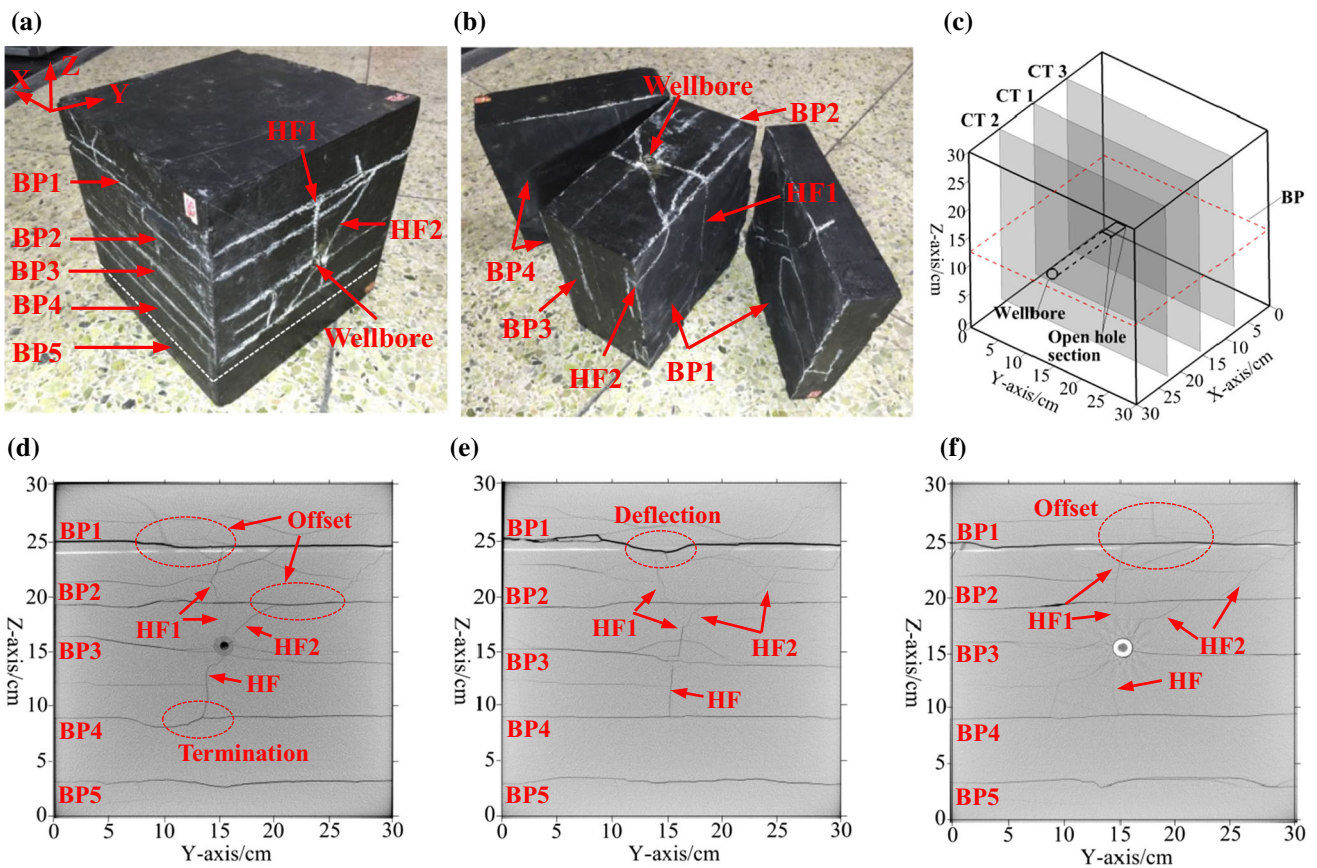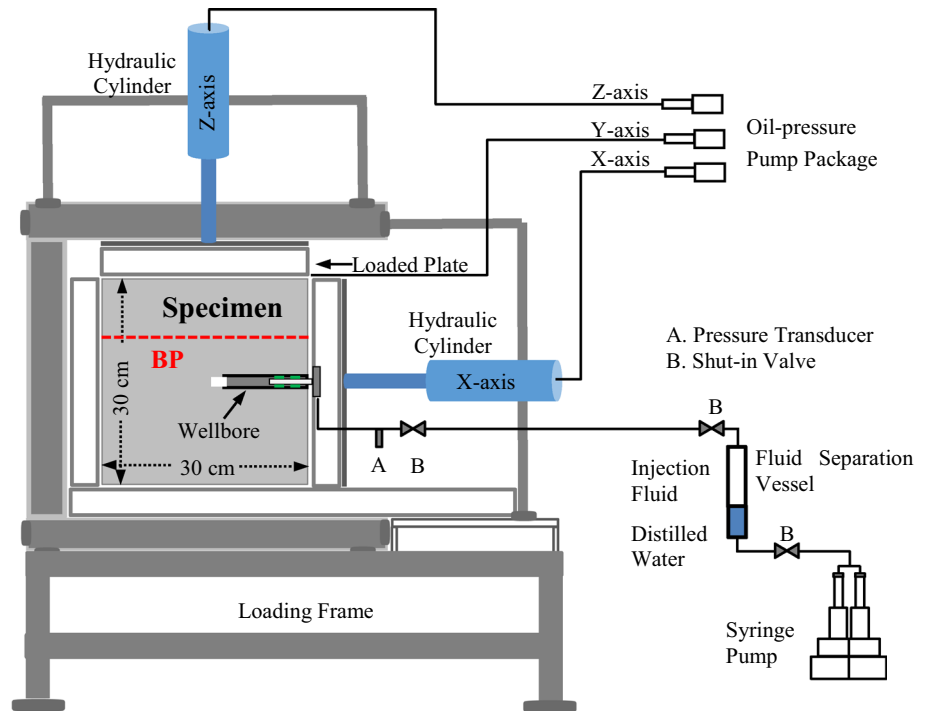

Fig. 4 HF geometry created in Specimen 1 when $\sigma_v = 30$ MPa, $\sigma_{h\text{max}} = 15$ MPa and $\sigma_{h\text{min}} = 10$ MPa, and $Q_t = 20.0$ mL/min: **a** surface HFs and BPs, **b** internal HFs and BPs, **c** CT scanning position indicators, **d** CT1: $X = 15.5$ cm (crossing the open hole), **e** CT2: $X = 23$ cm (crossing the steel tube), **f** CT3: $X = 8$ cm

Hanson et al. 1982; Teufel and Clark 1984; Thiercelin et al. 1989; Warpinski et al. 1982, 1998; Smith et al. 2001; Gu and Siebrits 2006; Fisher and Warpinski 2012; Chuprakov and Prioul 2015; Cohen et al. 2017). The in situ stress, fracture toughness, and Young's modulus contrasts and layer interfaces are the dominant parameters controlling HF height growth. Some mechanisms have also been proposed to explain the HF height containment, including the "composite layer effect," the "shear dampening," and the HF behavior at the layer interfaces (Barree and Winterfeld 1998; Warpinski et al. 1998; Cooke and Underwood 2001; Zhang et al. 2007; Zhang and Jeffrey 2012). These studies have mainly focused on the effects of mechanical parameter (stress, fracture toughness, and Young's modulus) variation between the adjacent formation layers in the vertical direction and the mechanical weakness of BPs and/or layer interfaces.

To focus on the important influence of multi-BP on the creation of complex HFN, a layered formation, in which all layers have the same mechanical parameters, was considered in previous numerical simulation studies (Zhou et al. 2016, b; Li et al. 2016). We previously performed a parameters sensitivity analysis that included vertical stress anisotropy, elastic anisotropy, strength anisotropy, and BP dipping angle. The results show that when various conditions were considered the HF growth and fluid flow paths would obviously differ. In this paper, further studies on the interaction between HF and multi-BP were carried out using both experimental and numerical methods. The parameters of vertical stress, BP permeability, BP density, fluid viscosity, and injection rate were mainly studied. The results can provide a more comprehensive understanding of HF height containment mechanisms in layered formations.

2 Experimental Studies

2.1 Experimental Procedure

Three cubic specimens with the dimensions of 300 mm × 300 mm × 300 mm were prepared for the fracturing experiments. The specimens were mined from an outcrop of the Longmaxi shale formation in the Sichuan Basin, China. X-ray diffraction analysis showed that the
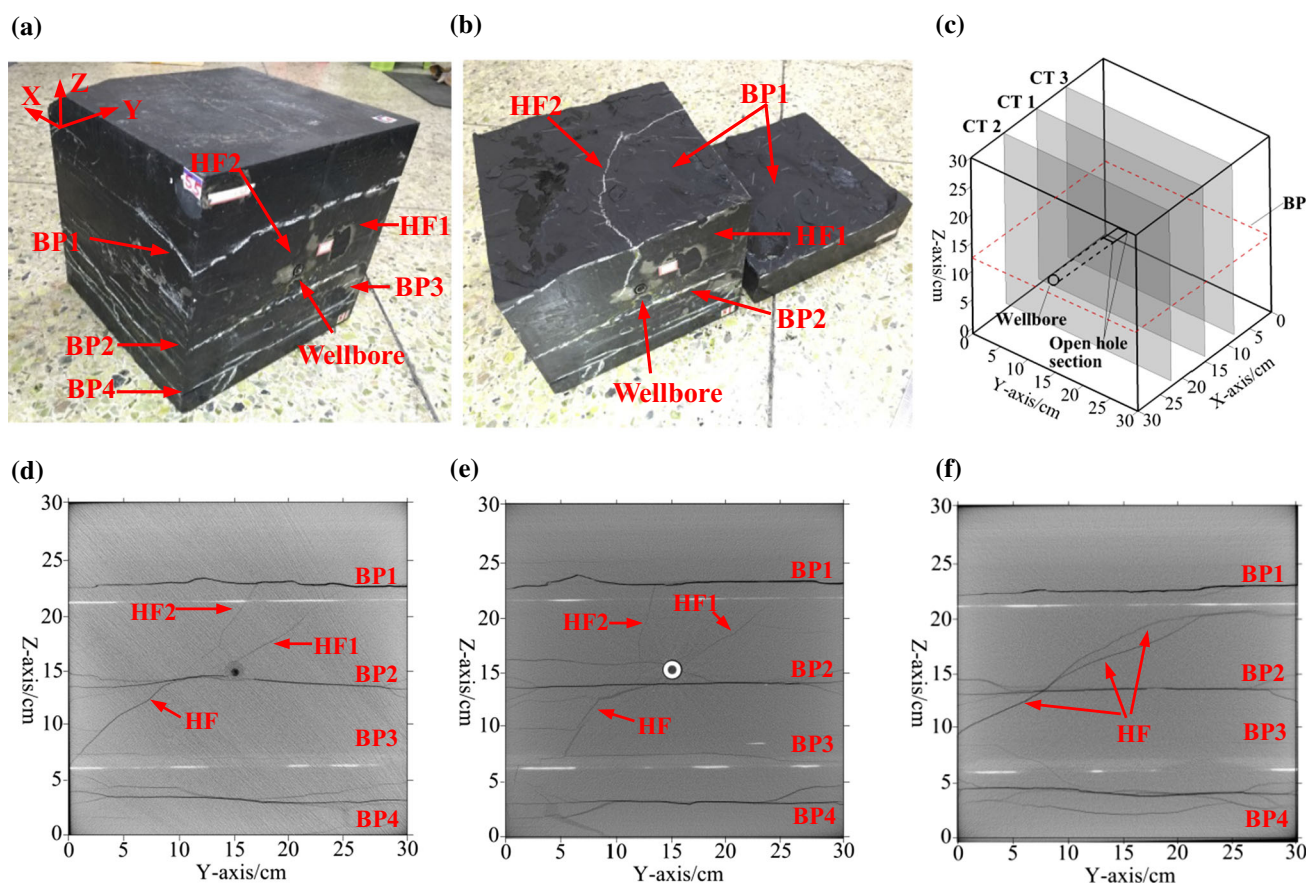

Fig. 5 HF geometry created in Specimen 2 when $\sigma_v = 15$ MPa, $\sigma_{hmax} = 15$ MPa and $\sigma_{hmin} = 10$ MPa, and $Q_t = 20.0$ mL/min: **a** surface HFs and BPs, **b** internal HFs and BPs, **c** CT scanning position indicators, **d** CT1: $X = 15.1$ cm (crossing the open hole), **e** CT2: $X = 22.5$ cm (crossing the steel tube), **f** CT3: $X = 8.5$ cm
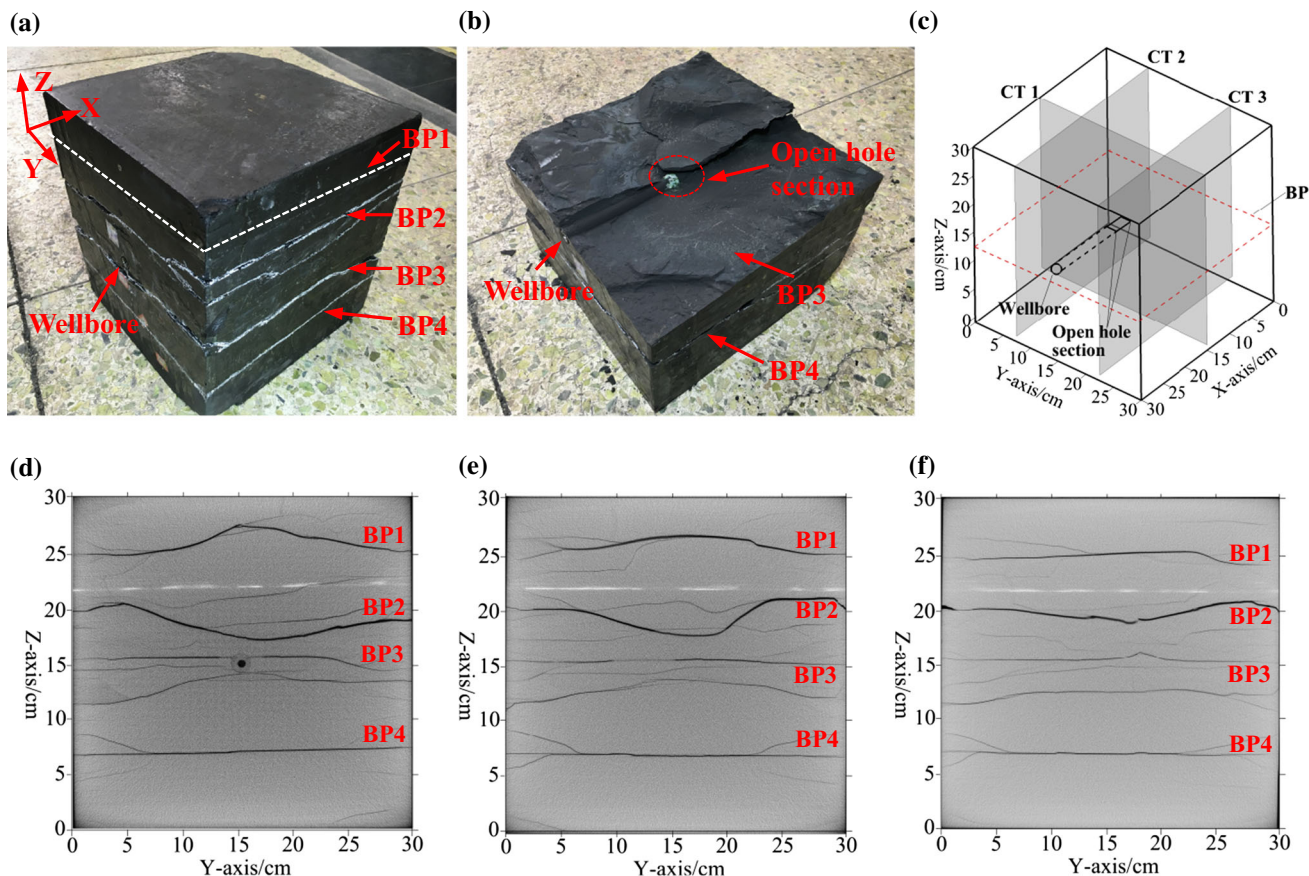
Fig. 6 HF geometry created in Specimen 3 when $\sigma_v = 15$ MPa, $\sigma_{h\max} = 15$ MPa and $\sigma_{h\min} = 10$ MPa, and $Q_t = 5.0$ mL/min: **a** surface HFs and BPs, **b** internal HFs and BPs, **c** CT scanning position indicators, **d** CT1: $X = 15$ cm (crossing the open hole), **e** CT2: $Y = 7.5$ cm, **f** CT3: $Y = 22.5$ cm

average mineral composition of the shale specimens was 50.6% quartz, 33.4% clay, 9.8% carbonatite, and 5.7% pyrite (by weight). Table 1 presents the properties of rock mechanics and the permeability of shale specimens. Note that the properties are significantly different in the directions parallel and perpendicular to the BPs. Some of the BPs in the shale specimens have extremely low tensile strength (0 MPa) but very high permeability (10^{-10} m^2). The preexisting BPs in the shale specimens can be determined by surface observation, as well as through the computerized tomography (CT) scanning technique (Guo et al. 2014; Zou et al. 2016a), as shown in Fig. 2. A central hole with 1.6 cm diameter and 16.5 cm depth was drilled along the BPs in the specimens for the horizontal wellbore modeling, and then a 13.5-cm steel tube with an external diameter of 1.5 cm and an internal diameter of 0.8 cm was placed into the hole. High-strength epoxy glue was used to bind the steel tube and the hole wall. An open hole section of 3 cm was eventually left to be pressurized by injecting the fracturing fluid through the wellbore.

Experiments were conducted using a true triaxial hydraulic fracturing system, as shown in Fig. 3. The BPs in the specimens were oriented horizontally on the loading frame, and the wellbore was oriented parallel to the X-axis direction. Vertical stress (σ_v) was applied in the Z-axis direction and was perpendicular to the BPs, whereas the maximum ($\sigma_{H\max}$) and minimum ($\sigma_{h\min}$) horizontal stresses were applied perpendicular (in Y-axis direction) and parallel to (in X-axis direction) the wellbore, respectively. In the present study, we examined the effects of vertical stress and pump rate; thus, $\sigma_{h\max} = 15$ MPa and $\sigma_{h\min} = 10$ MPa were fixed, and vertical stress was varied as $\sigma_v = 15, 30$ MPa; pump rate was varied as $Q_t = 5.0, 20.0$ mL/min. Slick-water fluid with viscosity $u = 2.5$ mPa s was injected into the wellbore. Yellow-green fluorescent agent was added into the fluid to better trace the HFs. After the experiments, we observed the external fracture morphology from the specimen surfaces based on the tracer distribution. Furthermore, CT scanning was used to reflect the internal fracture morphology. Finally, the specimens were split to reveal the HFs based on the tracer distribution and verified the reliability of the CT images. The steps mentioned were integrated to describe the overall geometry of the HF created in one
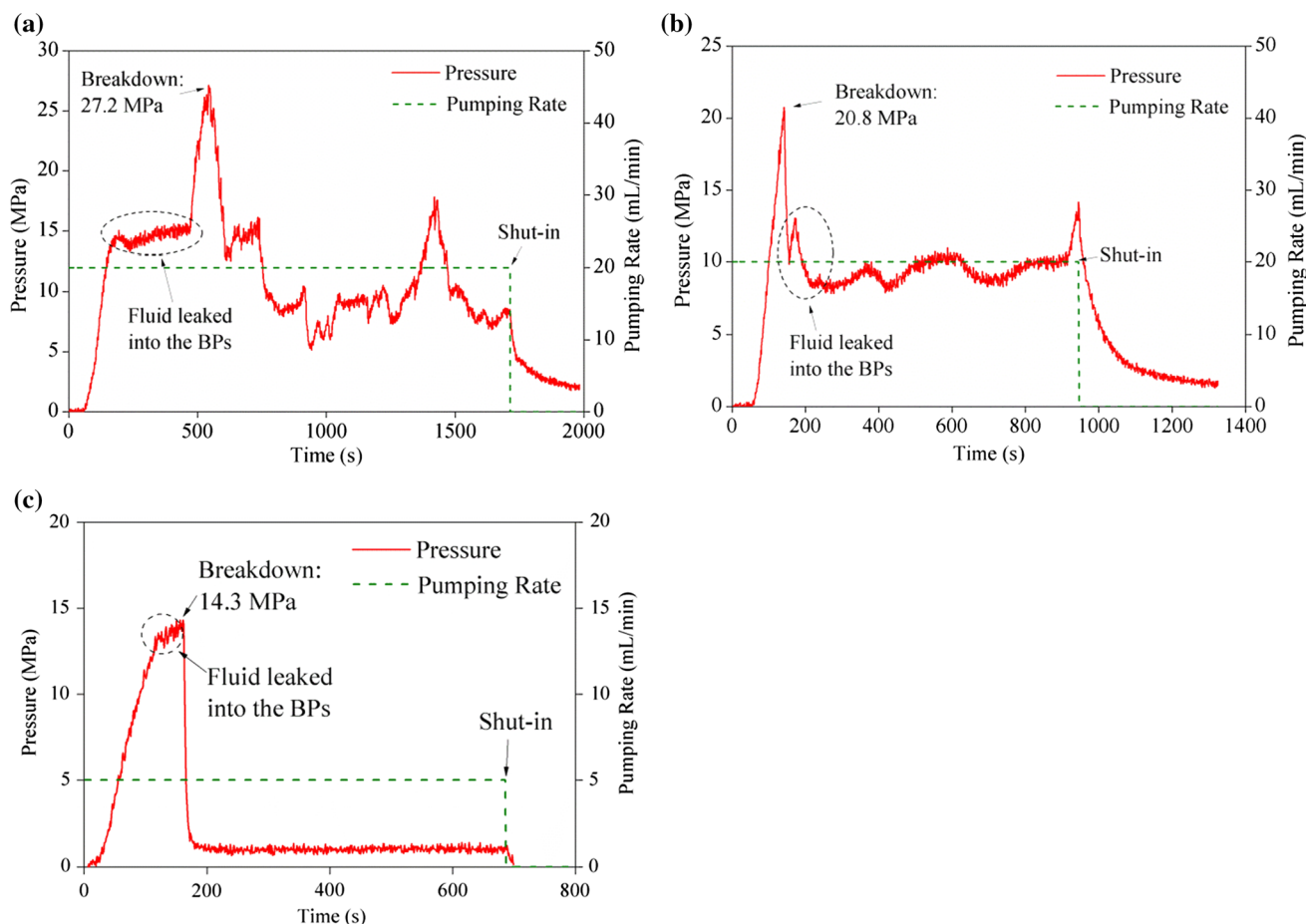
(a)

(b)

(c)

Fig. 7 Injection pressure versus time curves for the three specimens: **a** Specimen 1, **b** Specimen 2, and **c** Specimen 3

specimen. For details on the experiment procedure, the reader is referred to Guo et al. (2014) and Zou et al. (2016a).

2.2 Experimental Results and Analysis

2.2.1 HF Geometry result from the HF-BP Interaction

Figure 4 shows the resulting HF geometry in Specimen 1 that contained five visible BPs in the case of $\sigma_v = 30$ MPa, $\sigma_{hmax} = 15$ MPa and $\sigma_{hmin} = 10$ MPa, and $Q_t = 20.0$ mL/ min. One dominant HF with two branches was initiated nearly vertically and propagated along the wellbore (Fig. 4a, b). The interaction between HFs and BPs within Specimen 1 can be clearly seen in the CT scanning images at three different positions (Fig. 4c, d, e, and f). The HFs can directly penetrate through the BP3 near the wellbore and then terminate at the BP4 on the bottom of the wellbore. On top of the wellbore, one branch, namely HF1, penetrates through the BP2 and is then deflected into BP1. Afterward, HF1 can also re-initiate at the BP1, resulting in a step-over in the vertical direction. Other branches that

intersect with BP2, namely HF2, also cause the offset. In this experiment, all the four types of HF intersection with BP, including penetration, deflection, offset, and termination, were observed similar to previous studies (Thiercelin et al. 1987; Warpinski and Teufel 1987; Cooke and Underwood 2001; Zhang et al. 2007; Zhang and Jeffrey 2012; Zou et al. 2016b). Specimen 2 was hydraulically fractured under the same conditions as Specimen 1, but with lower vertical stress of $\sigma_v = 15$ MPa. In Specimen 2, one dominant HF with two branches propagates obliquely crossing the wellbore and it is then limited between BP1 and BP3, as shown in Fig. 5. The HF height created in Specimen 2 was obviously smaller than that created in Specimen 1. Specimen 3 was hydraulically fractured under the same conditions as Specimen 2 but with a lower pump rate of $Q_t = 5.0$ mL/min. In Specimen 3, no vertical HF can be observed, as shown in Fig. 6 mainly because the HF was initiated horizontally and propagated along the BP3 that connects with the open hole. This result indicated that a lower pumping rate can promote HF growth along the BPs.

Fig. 8 Model construction for a layered formation containing multiple BPs: **a** model mesh, **b** equally spaced BPs which were predefined in the model (*d* is the BP spacing)
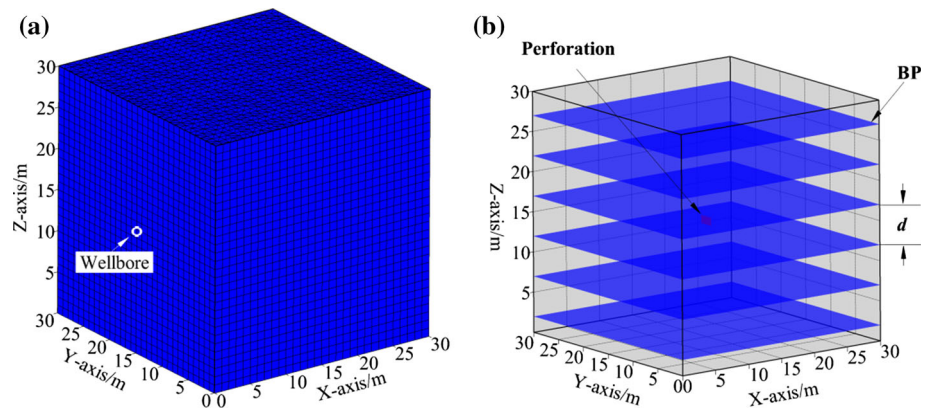

Table 2 Parameters set for the numerical simulations

Parameter	Symbol	Units	Value
Max. horizontal stress	$\sigma_{H\max}$	MPa	15
Min. horizontal stress	$\sigma_{h\min}$	MPa	10
Vertical stress	σ_{v}	MPa	12, 14, 16, 20
Initial pore pressure	p_{int}	MPa	0
Tensile strength perpendicular to BP	T_{0v}	MPa	2
Tensile strength parallel to BP	T_{0h}	MPa	6.7
Cohesion perpendicular to BP	S_{0v}	MPa	16
Cohesion parallel to BP	S_{0h}	MPa	4
Frictional angle perpendicular to BP	φ_{h}	MPa	45
Frictional angle parallel to BP	φ_{v}	MPa	25
BP permeability	k_{BP}	10^{-12} m^2	10^{-7}, 0.1, 5, 100
BP spacing	d	m	1, 3, 5, 7
Pumping rate	Q_{t}	m^3/s	0.01, 0.05, 0.1
Fluid viscosity	μ	mPa·s	1, 2.5, 10

2.2.2 Injection Pressure Analysis

The details of the HF growth geometries were also reflected in the injection pressure responses. In Fig. 7, the time dependence of the injection pressures is recorded for the three experiments conducted under different conditions. Notably, the injection pressure curve patterns were significantly different for the three specimens. As the fracturing fluid was pumped into the wellbore, the injection pressure rapidly increased. For Specimen 1, when the injection pressure reached approximately 14.5 MPa, the BP3 that connected with the open hole was initiated partially; afterward, a large amount of fracturing fluid leaked into the BP3. Given that a large vertical stress of $\sigma_v = 30$ MPa was applied on Specimen 3, the complete opening of BP3 became unlikely. When the open space of BP 3 was completely filled with fracturing fluid, a high injection pressure can then be built up rapidly until pressure breakdown of 27.2 MPa and after it declined sharply (Fig. 7a). A HF was initiated vertically from the open hole. The vertically growing HF intersects with the BPs on the

top and bottom of the wellbore, which then causes the extension pressure to fluctuate remarkably.

For Specimen 2, no BP connects with the open hole directly, so the injection pressure can increase rapidly until the breakdown pressure of 20.2 MPa (Fig. 7b). This high injection pressure enables the HF to initiate vertically and to penetrate through the BP2 on the bottom of the wellbore. When the vertically growing HF encounters BP1 that has a large width, a massive amount of fracturing fluid leaked into BP3, which terminates the HF at BP3. In general, the extension pressure variation for Specimen 2 was not as evident as compared with that of Specimen 1. This finding is mainly attributed to the number of BP in Specimen 2, which the vertically growing HF can encounter that is less than that in Specimen 1. Meanwhile, the HF geometry created in Specimen 1 is more complex.

The breakdown pressure of Specimen 3 was 14.3 MPa, which was lower than those of Specimens 1 and 2 (Fig. 7c). For Specimen 3, the use of a lower pumping rate established a lower injection pressure, which was insufficient for promoting the HF to penetrate through the BP3
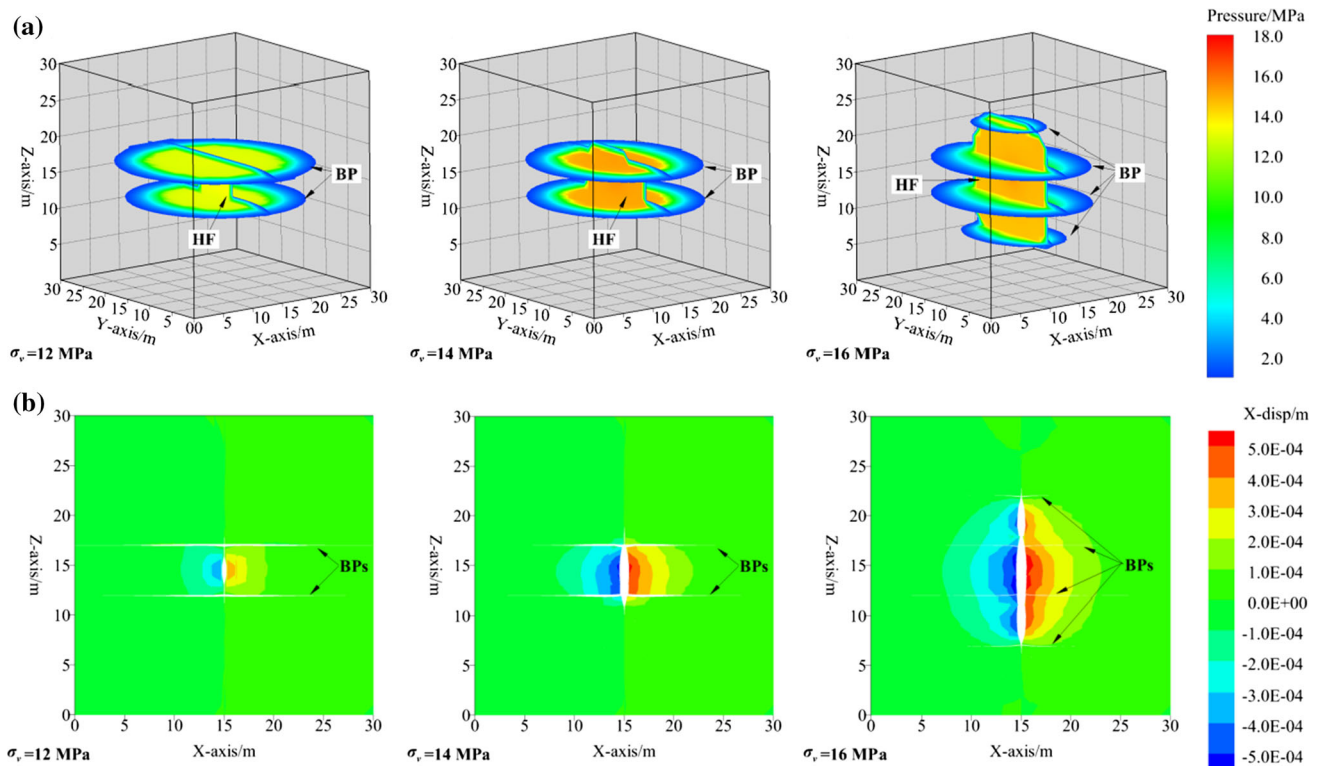
Fig. 9 HF patterns for different vertical stresses in the case of $k_{BP} = 5.0 \times 10^{-12}$ m², $d = 5.0$ m, $Q_t = 0.05$ m³/s, $u = 2.5$ mPa s, **a** fluid pressure distributions, **b** displacement profiles in the X-axis at $y = 15$ m

that has a huge opening. Thus, once the BP3 in Specimen 3 was initiated, all the injected fracturing fluid would leak into BP3, resulting in a very low extension pressure. The injection pressure was maintained at a low value until the fracturing fluid reached the specimen surfaces.

3 Numerical Modeling

3.1 Model Description

Numerical simulations of HF growth in a layered formation were performed using the 3D complex fracturing model proposed in our previous studies (Zhou et al. 2016, b, c; Li et al. 2016). This model coupled rock deformation and fluid flow inside the HF based on the DEM and FEM. In this model, rock mass was considered impermeable, transversely isotropic and linearly elastic (Zou et al. 2016b), whereas, for the DEM, the rock mass was necessarily divided into several block elements bonded by virtual springs, which transferred the interaction forces among blocks. The motion of each block was determined by the magnitude of the resultant unbalanced force that acted on it. The joint elements inserted between all contacting blocks build a continuous flow network (called DFN) for generating HFs. The size, shape, and orientation of this

DFN depended on the predefined planes of the BPs. The fluid pressure distribution inside the DFN was calculated by the FEM. The fluid pressure was then exerted on the surrounding blocks, resulting in deformations and changes in the stress states at the block contacts. A HF is generated if the stress level at the interface between two blocks exceeds a threshold value either in tension (maximum tensile stress criterion) or in shear (Coulomb criterion). Details of basic theory and the governing equations of this
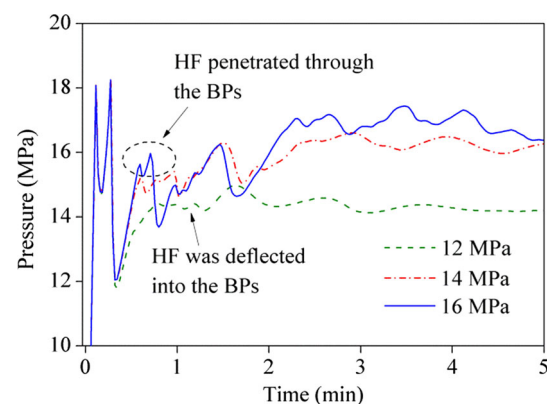

Fig. 10 Injection pressure versus time curves under different vertical stresses in the case of $k_{BP} = 5.0 \times 10^{-12}$ m², $d = 5.0$ m, $Q_t = 0.05$ m³/s, $u = 2.5$ mPa s
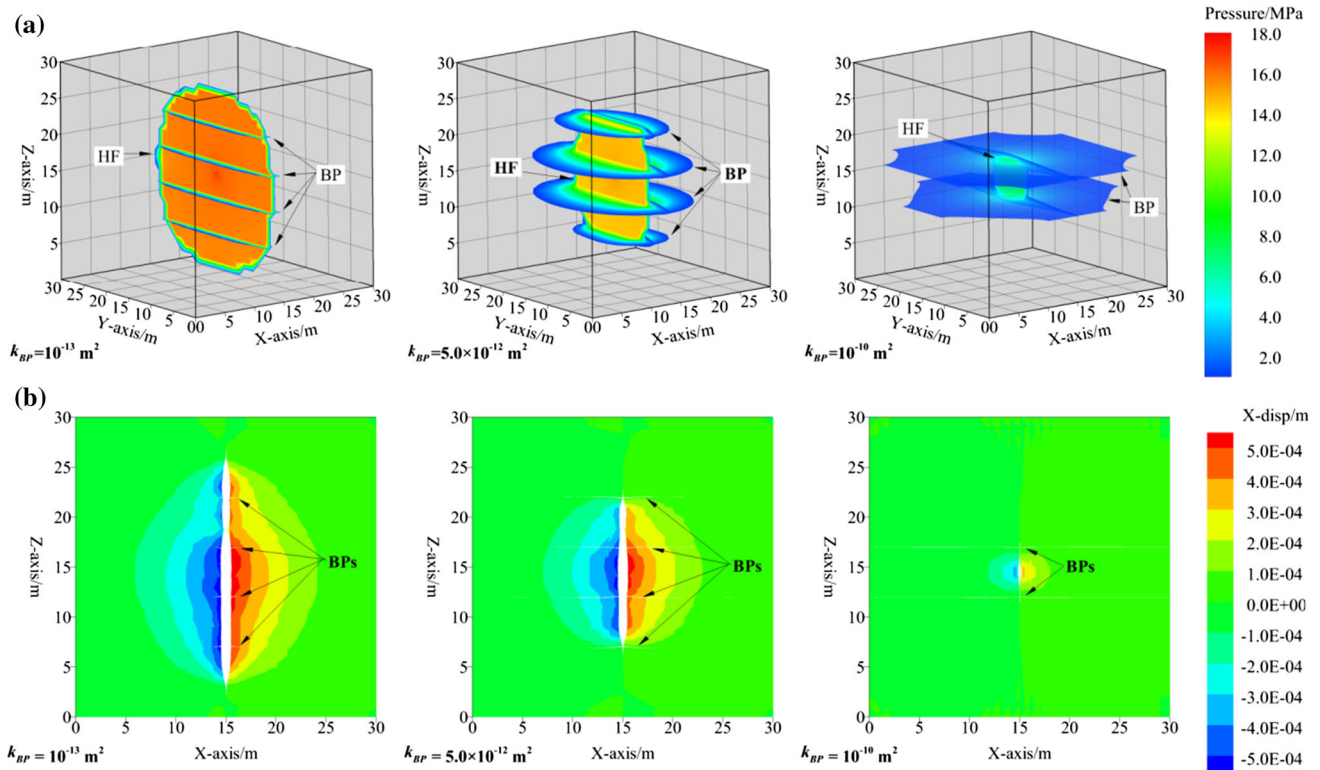
(a)

(b)

Fig. 11 HF patterns for different k_{BP} values in the case of $\sigma_v = 20$ MPa, $d = 5.0$ m, $Q_t = 0.05$ m³/s, $u = 2.5$ mPa s, **a** fluid pressure distributions, **b** displacement profiles in the X-axis at $y = 15$ m

model are found in our previous works (Zhou et al. 2016, b, c; Li et al. 2016).

To explore the interaction between the HF and the multiple BPs, a multi-layered formation model measuring 30 m × 30 m × 30 m in size was established, as shown in Fig. 8. In the model meshing process, the BP planes are treated as predetermined edges. Figure 8a shows the model mesh with the triangular prism element, which has an average edge length of 1 m. The choice of element size was tested and found to be sufficient to provide accurate numerical results (Zou et al. 2016b). The multi-BP contained in the model was equally spaced, and the formation was divided into multi-layer, as shown in Fig. 8b. The minimum (σ_{hmin}) and maximum (σ_{hmax}) horizontal stresses, as well as the vertical stress (σ_v), were set in the directions parallel to the x-, y-, and z-axes, respectively. One perforation was located at the coordinate of $x = 15$ cm, $y = 15$ cm, and $z = 15$ cm, where the injection point of the fracturing fluid was found.

3.2 Modeling Results and Analysis

Based on the configuration shown in Fig. 8, we primarily investigated the effects of vertical stress, BP permeability, BP density, fluid viscosity, and injection rate on the HF growth geometry in a layered formation. The parameters
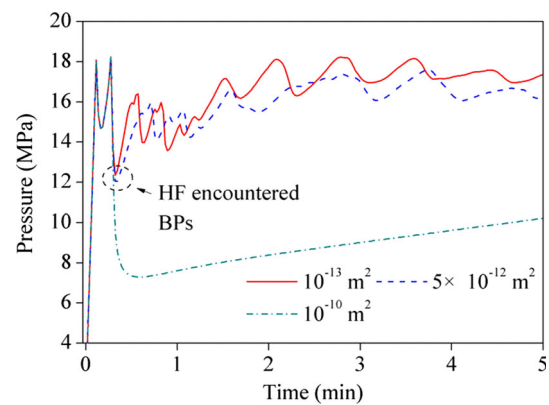

Fig. 12 Injection pressure versus time curves for different k_{BP} values in the case of $\sigma_v = 20$ MPa, $d = 5.0$ m, $Q_t = 0.05$ m³/s, and $u = 2.5$ mPa s

used in the numerical simulations are presented in Tables 1 and 2. We determined the influence of each parameter when its value varied within a range, whereas all other parameters remained constant. The initial pore pressure was considered zero.

3.2.1 Effect of Vertical Stress

Figure 9 shows the resulting HF patterns for different vertical stresses σ_v in the case of $k_{BP} = 5.0 \times 10^{-12}$ m²,
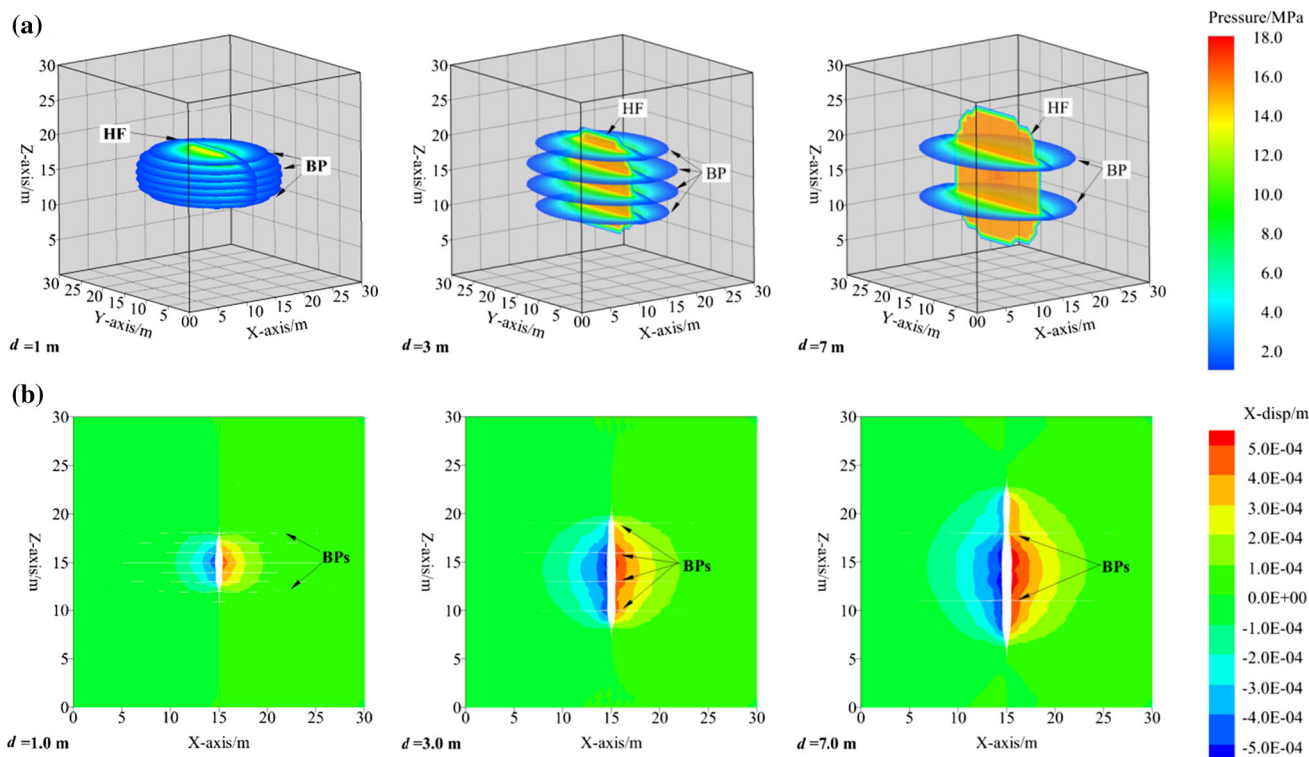
(a)

(b)

Fig. 13 HF patterns for different BP spacing d in the case of $\sigma_v = 20$ MPa, $k_{BP} = 5.0 \times 10^{-12}$ m^2, $Q_t = 0.05$ m^3/s and $u = 2.5$ mPa s, **a** fluid pressure distributions, **b** displacement profiles in the X-axis at $y = 15$ m

$d = 5.0$ m, $Q_t = 0.05$ m^3/s, $u = 2.5$ mPa s. Evidently, the vertically initiated HF was deflected into the two BPs on the top and bottom of the perforation when $\sigma_v = 12$ MPa and $\sigma_v = 14$ MPa, whereas it can penetrate through multi-BP when $\sigma_v = 16$ MPa, as shown in Fig. 9a. Note that the HF of a narrower width and a larger area of opened BPs was present when $\sigma_v = 12$ MPa compared with the case of $\sigma_v = 14$ MPa. This finding was well reflected by the injection pressure curves, as shown in Fig. 10. Considering that the HF can be deflected into the BPs easily and a large fracturing fluid leaked into the BPs, the injection pressure was relatively low, thereby narrowing the fracture width. When $\sigma_v = 14$ MPa, the HF growth along the BPs hardened, thus, the injection pressure evidently increased. Although the fracturing fluid can still leak into the BPs, the HF diversion into the BPs when $\sigma_v = 16$ MPa was difficult. Therefore, a much higher injection pressure is necessary to drive the HF to grow vertically.

3.2.2 Effect of BP Permeability

The effect of BP permeability was examined in the case of $\sigma_v = 20$ MPa, $d = 5.0$ m, $Q_t = 0.05$ m^3/s, $u = 2.5$ mPa s. Under the used parameters, the vertically initiated HF was unlikely to open the BPs, but the amount of fracturing fluid evidently rose as BP permeability increased, as shown in
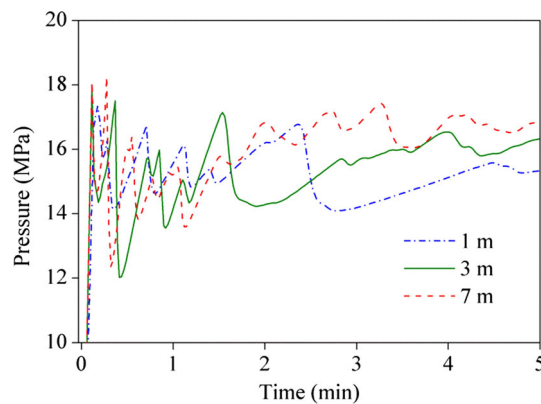

Fig. 14 Injection pressure versus time curves for different BP spacing d in the case of $\sigma_v = 20$ MPa, $k_{BP} = 5.0 \times 10^{-12}$ m^2, $Q_t = 0.05$ m^3/s and $u = 2.5$ mPa s

Fig. 11. All the fracturing fluid would leak into the BPs after the HF encountered the BPs of a permeability of 10^{-10} m^2. This result made the resulting HF very narrow and short. Given that the fracturing fluid can easily penetrate into the BPs with a very high permeability, the injection pressure declined sharply after the HF encountered the BPs and was maintained at a very low value, as shown in Fig. 12. The injection pressure curve pattern was similar to that in Fig. 7c.

3.2.3 Effect of BP Density

The density of BP is characterized by the BP spacing d. Figure 13 shows the resulting HF patterns for different BP spacing d in the case of $\sigma_v = 20$ MPa, $k_{BP} = 5.0 \times 10^{-12}$ m², $Q_t = 0.05$ m³/s and $u = 2.5$ mPa s. Notably, the HF height was obviously reduced as the BP spacing d decreased. The HF height was about 6 m when $d = 1$ m, and it was about 17 m when $d = 7$ m. A smaller d means that denser BPs exist in a formation. The possibility of the HF intersection with the BPs will increase as the density of BP increases. Meanwhile, more fracturing fluid will leak into the BPs. When $d = 1$ m, one BP connected with the perforation, so the breakdown pressure was 17.4 MPa which was lower than that of 18.1 MPa when no BPs exist nearby the perforation (e.g., $d = 3$ m), as shown in Fig. 14. The injection pressure is generally lower when more BPs exist in the formation. As a whole, the "composite layer effect" will be more evident when denser BPs exist in a formation, which limits the HF height growth.

3.2.4 Effect of Pumping Rate

Figures 15 and 16 show the resulting HF patterns for different Q_t values in the case of $k_{BP} = 5.0 \times 10^{-12}$ m², $d = 5$ m and $u = 2.5$ mPa s, but two different vertical stresses σ_v. For a higher vertical stress of $\sigma_v = 20$ MPa, the HF would grow vertically without opening the BPs across the used pumping rates, as shown in Fig. 15. For a lower vertical stress of $\sigma_v = 14$ MPa, the vertically growing HF can penetrate through and open the BPs at a high pumping rate of $Q_t = 0.1$ m³/s. Note that using a low pumping rate of $Q_t = 0.01$ m³/s would initiate the HF at a lower breakdown pressure of 17.3 MPa and grow at a lower extension pressure, as shown in Fig. 17. When $Q_t = 0.01$ m³/s was used, almost all of the fracturing fluid would leak out from the vertical HF into the BPs, which was well indicated by the sharply reduced injection pressure, thereby terminating the HF at the BPs. Furthermore, the extension pressures were lower and fluctuated weakly when the HF penetrated into the BPs, as shown in Fig. 17. The result was consistent with the experimental result shown in Sect. 2.2.
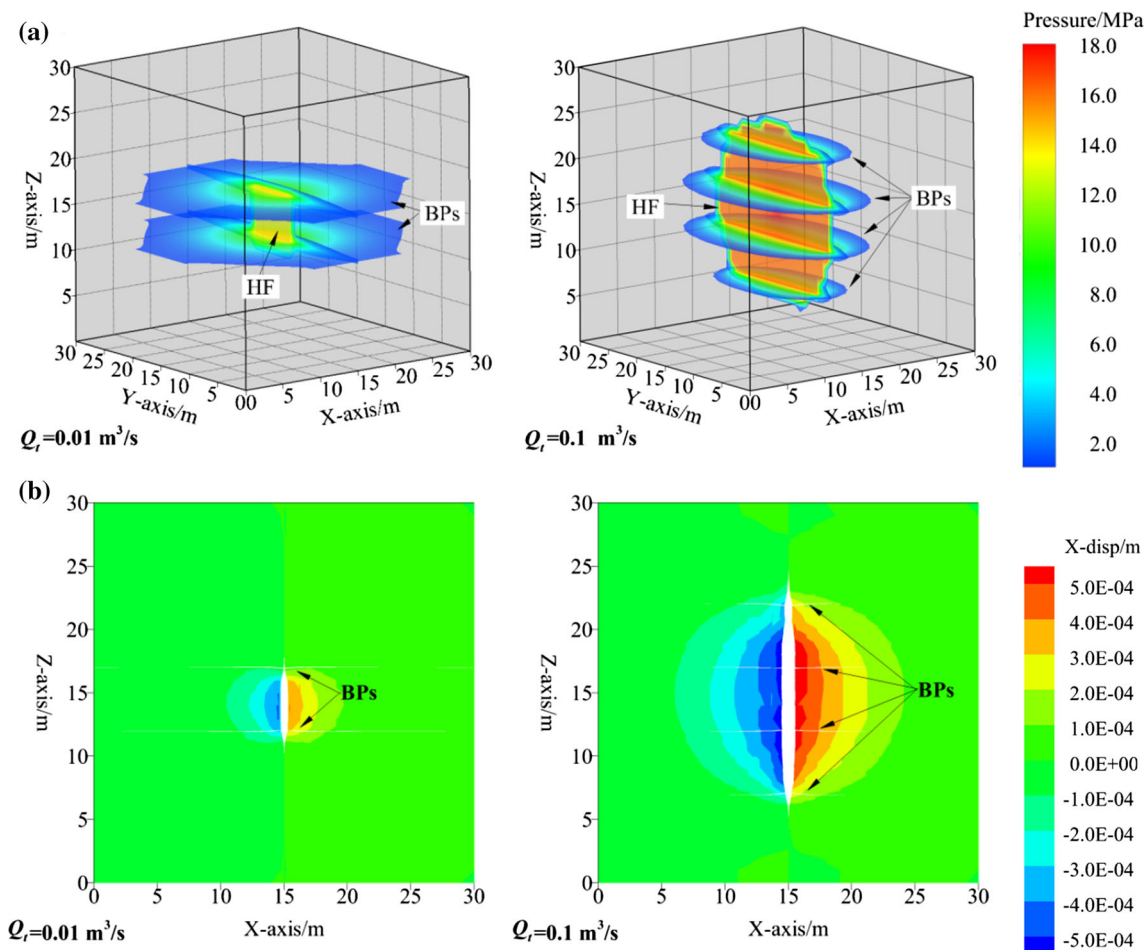

Fig. 15 HF patterns for different Q_t values in the case of $\sigma_v = 20$ MPa, $k_{BP} = 5.0 \times 10^{-12}$ m², $d = 5$ m, and $u = 2.5$ mPa s, **a** fluid pressure distributions, **b** displacement profiles in X-axis at $y = 15$ m

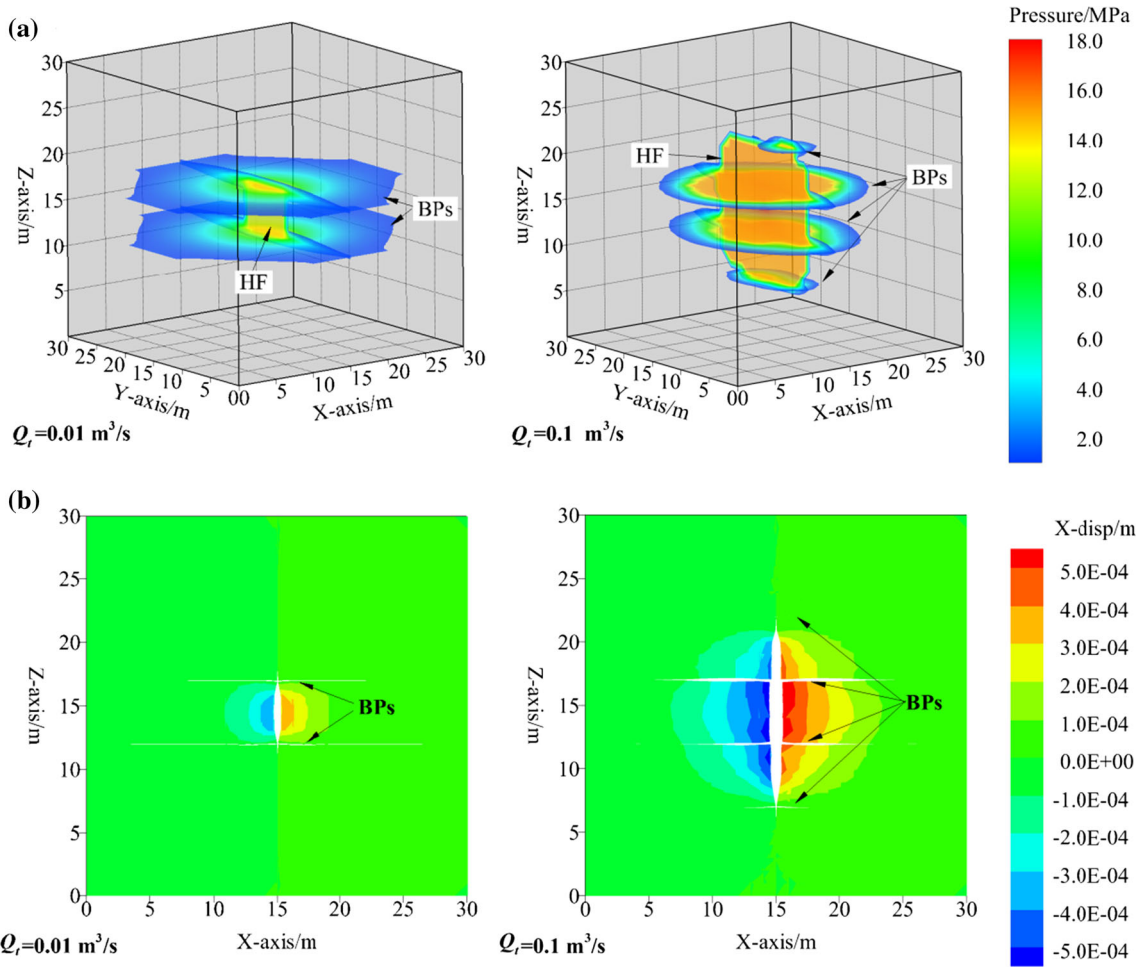**Fig. 16** HF patterns for different Q_t values in the case of $\sigma_v = 14$ MPa, $k_{BP} = 5.0 \times 10^{-12}$ m², $d = 5.0$ m and $u = 2.5$ mPa s, **a** fluid pressure distributions, **b** displacement profiles in the X-axis at $y = 15$ m
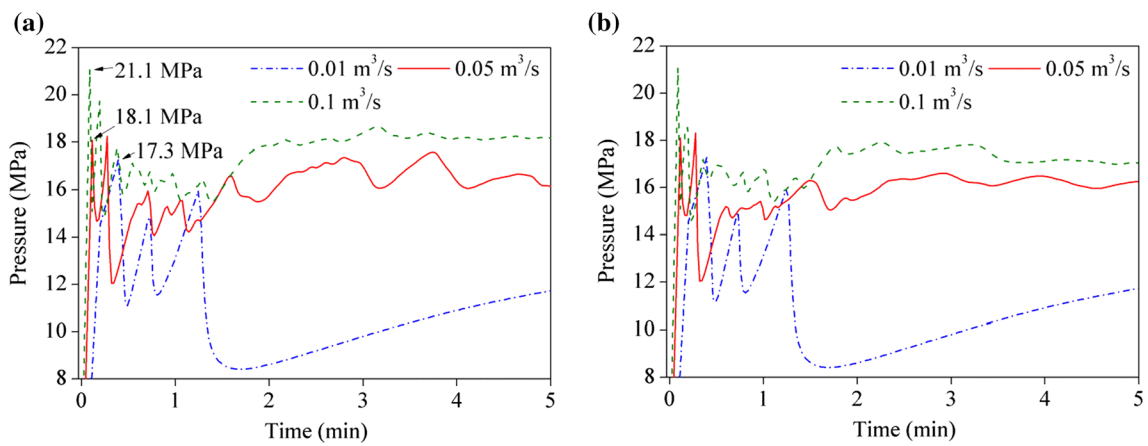

Fig. 17 Injection pressure versus time curves for different Q_t values in the case of $k_{BP} = 5.0 \times 10^{-12}$ m², $d = 5.0$ m and $u = 2.5$ mPa s, **a** $\sigma_v = 20$ MPa, **b** $\sigma_v = 14$ MPa

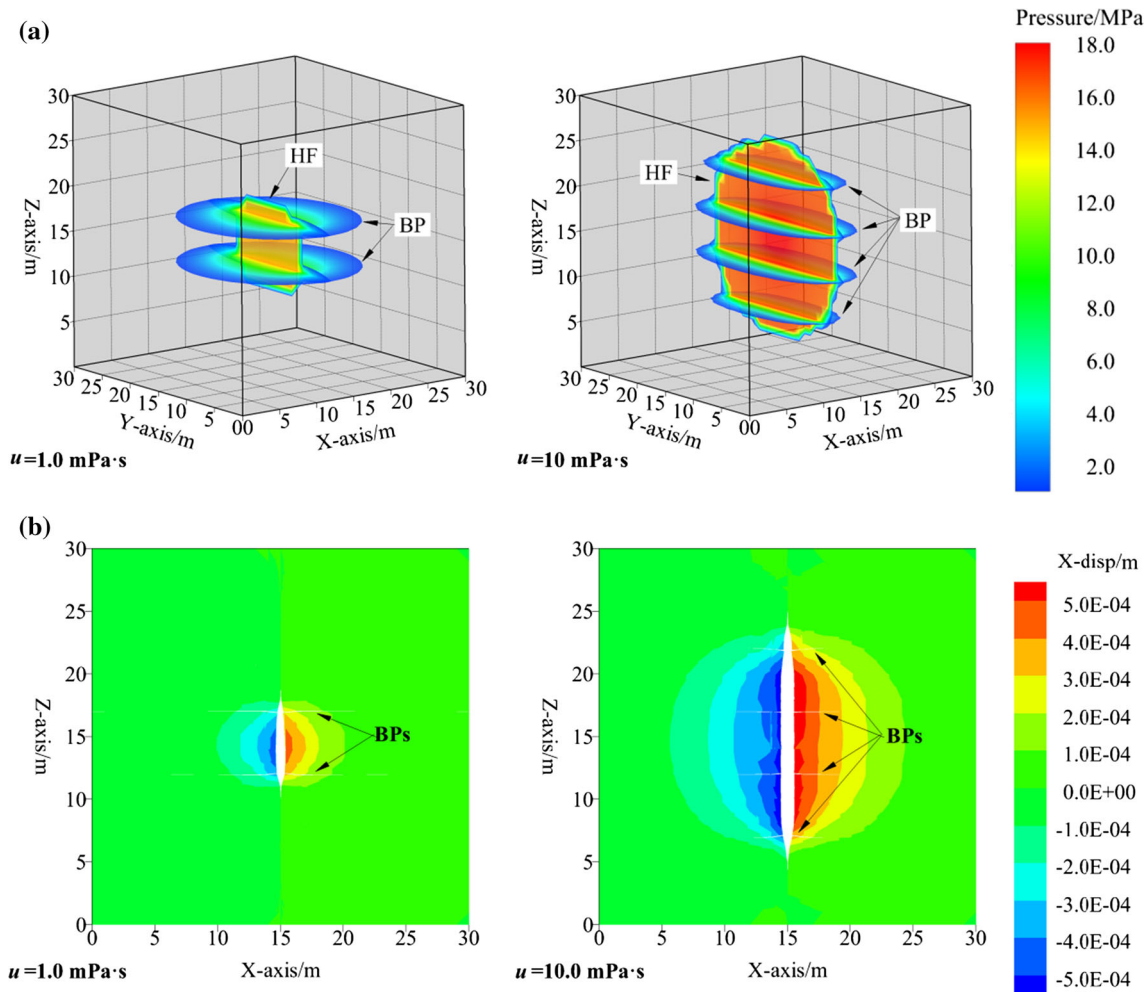**Fig. 18** HF patterns for different fluid viscosities in the case of $\sigma_v = 20$ MPa, $k_{BP} = 5.0 \times 10^{-12}$ m^2, $d = 5.0$ m, and $Q_t = 0.05$ m^3/s, **a** fluid pressure distributions, **b** displacement profiles in the X-axis at $y = 15$ m

3.2.5 Effect of Fluid Viscosity

The vertically growing HF will terminate at the BPs on the top and bottom of the perforation when a low-viscosity fluid of $u = 1.0$ mPa s was used under either a high or low σ_v, as shown in Figs. 18 and 19. Lower breakdown and extension pressures were also present when a lower-viscosity fluid was used due to the large leak-off volume of fracturing fluid, as shown in Fig. 20. Otherwise, the use of a higher-viscosity fluid enables the HF initiation and growth at a higher injection pressure and promotes the HF to penetrate through the BPs, especially under the low σ_v, as shown in Fig. 19. This finding confirms that high-viscosity fluid is conducive to the HF crossing the preexisting discontinuities (e.g., natural fractures and bedding planes), whereas low-viscosity fluid tends to penetrate into the preexisting discontinuities (Beugelsdijk et al. 2000; Zou et al. 2016a).

4 Conclusions

In this study, we explored the height growth law of HF and injection pressure responses in a layered formation, which contains multi-high-permeability BPs through experimental and numerical methods. Both experimental and numerical results show that the vertically growing HF is likely to be limited by the multi-high-permeability BPs. When the vertically growing HF intersects with the multi-high-permeability BPs, a sharply reduced injection pressure will be present. If a low pumping rate or viscosity fluid is used, creating a high HF is difficult because most fluids filtrate into the BPs. This result obviously reduces the rate of pressure build up, which limits HF growth. Otherwise, a higher pumping rate and/or a higher viscosity will reduce the leak-off time and fluid volume, but increase the injection pressure to drive the HF to grow and penetrate through the BPs. The HF–BP interaction process can be reflected by
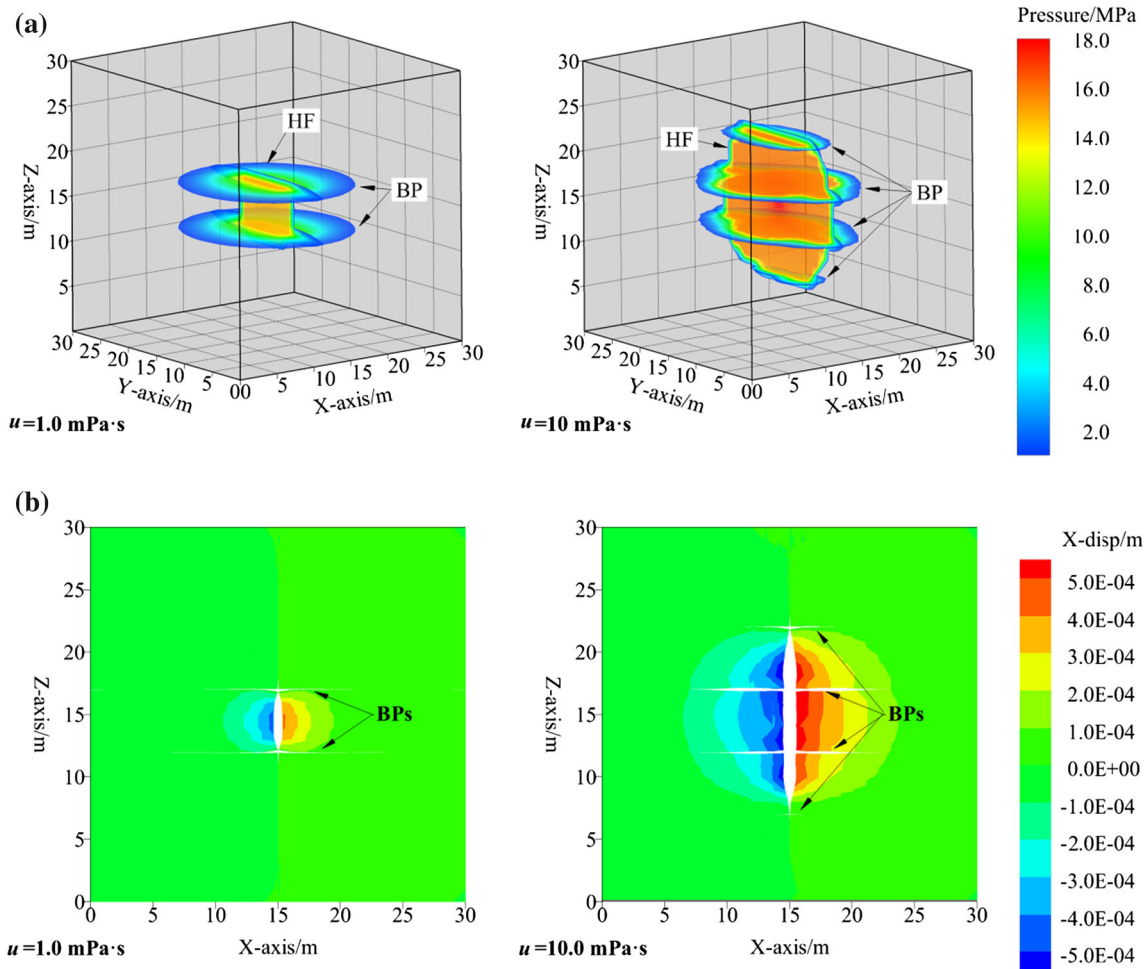
Fig. 19 HF patterns for different fluid viscosities in the case of $\sigma_v = 14$ MPa, $k_{BP} = 5.0 \times 10^{-12}$ m^2, $d = 5.0$ m, and $Q_t = 0.05$ m^3/s, **a** fluid pressure distributions, **b** displacement profiles in the X-axis at $y = 15$ m
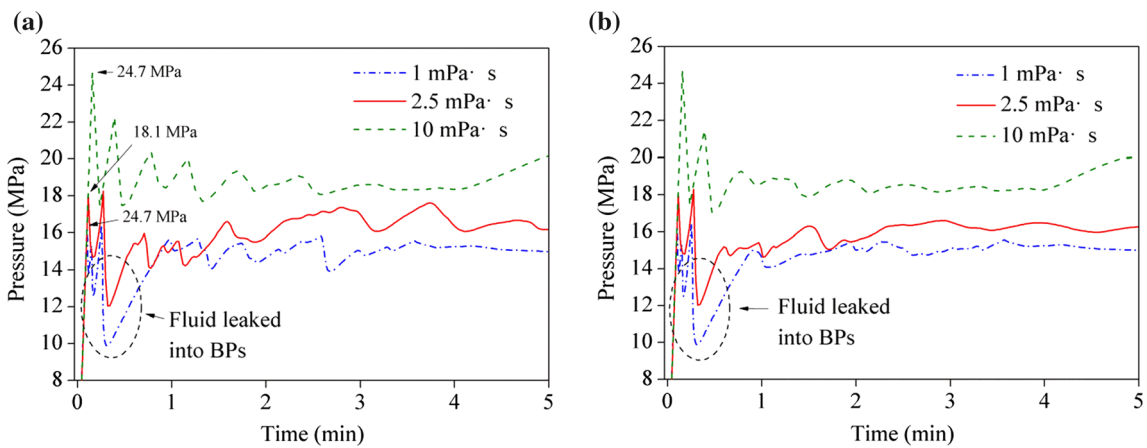

Fig. 20 Pumping pressure versus time curves for different fluid viscosities in the case of $k_{BP} = 5.0 \times 10^{-12}$ m^2, $d = 5.0$ m, and $Q_t = 0.05$ m^3/s, **a** $\sigma_v = 20$ MPa, **b** $\sigma_v = 14$ MPa

the injection pressure curve recorded during a fracturing of the layered formation. To obtain more accurate understanding of the dynamic interaction between the HF and multi-BP during a fracturing experiment in laboratory, the acoustic emission monitoring should be used in future studies (Stanchits et al. 2012, 2015).

References

Barree RD, Winterfeld PH (1998) Effects of shear planes and interfacial slippage on fracture growth and treating pressure. In: SPE annual technical conference and exhibition, society of petroleum engineers

Beugelsdijk LJL, de Pater CJ, Sato K (2000) Experimental hydraulic fracture propagation in a multi-fractured medium. In: SPE Asia Pacific conference on integrated modeling for asset management, society of petroleum engineers

Chuprakov D, Prioul R (2015) Hydraulic fracture height containment by weak horizontal interfaces. In: SPE hydraulic fracturing technology conference, society of petroleum engineers

Cohen CE, Kresse O, Weng XW (2017) Stacked height model to improve fracture height growth prediction and simulate interactions with multi-layer DFNs and ledges at weak zone interfaces. In: SPE hydraulic fracturing technology conference, society of petroleum engineers

Cooke ML, Underwood CA (2001) Fracture termination and stepover at bedding interfaces due to frictional slip and interfaceopening. J Struct Geol 23(2–3):223–238

Daneshy AA (1978) Hydraulic fracture propagation in layered foramtions. SPE J 18(1):33–41

Fisher K, Warpinski NR (2012) Hydraulic fracture height growth: real data. In: SPE annual technical conference and exhibition, society of petroleum engineers

Gu HG, Siebrits E (2006) Effect of formation modulus contrast on hydraulic fracture height containment. In: SPE international oil and gas conference and exhibition, society of petroleum engineers

Guo TK, Zhang SC, Qu ZQ, Zhou T, Xiao YS, Gao J (2014) Experimental study of hydraulic fracturing for shale by stimulated reservoir. Fuel 128:373–380

Hanson ME, Anderson GD, Shaffer RJ (1982) Some effects of stress, friction, and fluid flow on hydraulic fracturing. SPE J 22(3):321–332

Li H, Zou YS, Valko P, Ehlig-Economides C (2016) Hydraulic fracture height predictions in laminated shale formations using finite element-discrete element method. In: SPE hydraulic fracturing technology conference, society of petroleum engineers

Smith MB, Bale AB, Britt LK, Klein HH, Siebrits E, Dang X (2001) Layered modulus effects on fracture propagation, proppant placement, and fracture modeling. In: SPE annual technical conference and exhibition, Society of Petroleum Engineers

Stanchits S, Surdi A, Edelman E, Suarez-Rivera R (2012) Acoustic emission and ultrasonic transmission monitoring of hydraulic fracture propagation in heterogeneous rock samples. In: 46th U.S. rock mechanics/geomechanics symposium, American rock mechanics association

Stanchits S, Burghardt J, Surdi A (2015) Hydraulic fracturing of heterogeneous rock monitored by acoustic emission. Rock Mech Rock Eng 48(6):2513–2527

Teufel LW, Clark JA (1984) Hydraulic fracture propagation in layered rocks: experimental studies of fracture containment. Soc Pet Eng J 24(1):19–32

Thiercelin M, Jeffrey RG, Ben Naceur K (1989) Influence of fracture toughness on the geometry of hydraulic fractures. SPEPE 4(4):435–442

Thiercelin M, Roegiers JC, Boone TJ, Ingraffea AR (1987) An investigation of the material parameters that govern the behavior of fractures approaching rock interfaces. In: 6th International congress of rock mechanics, International Society for Rock Mechanics

Warpinski NR, Teufel LW (1987) Influence of geologic discontinuities on hydraulic fracture propagation. J Pet Technol 39(2):209–220

Warpinski NR, Schmidt RA, Northrop DA (1982) In-situ stress: the predominant influence on hydraulic fracture containment. JPT 34(3):653–664

Warpinski NR, Branagan PT, Peterson RE, Wolhart SL (1998) An interpretation of M-site hydraulic fracture diagnostic results. In: SPE rocky mountain regional/low-permeability reservoir symposium, society of petroleum engineers

Zhang X, Jeffrey RG (2012) Fluid-driven multiple fracture growth from a permeable bedding plane intersected by an ascending hydraulic fracture. J Geophys Res 117:B12402

Zhang X, Jeffrey RG, Thiercelin M (2007) Deflection and propagation of fluid-driven fractures at frictional bedding interfaces: a numerical investigation. J Struct Geol 29(3):396–410

Zhou T, Zhang SC, Zou YS, Ma XF, Li Ning, Hao SY, Zheng YH (2016) A study of hydraulic fracture geometry concerning complex geologic condition in shales. In: IPTC international petroleum technology conference

Zou YS, Zhang SC, Zhou T, Zhou X, Guo TK (2016a) Experimental investigation into hydraulic fracture network propagation in gas shales using CT scanning technology. Rock Mech Rock Eng 49:33–45

Zou YS, Ma XF, Zhang SC, Zhou T, Li H (2016b) Numerical Investigation into the Influence of bedding plane on hydraulic fracture network propagation in shale formations. Rock Mech Rock Eng 49:3597–3614

Zou YS, Zhang SC, Ma XF, Zhou T, Zeng B (2016c) Numerical investigation of hydraulic fracture network propagation in naturally fractured shale formations. J Struct Geol 84:1–13